ADVANCES IN ATMOSPHERIC SCIENCES, VOL. 25, NO. 6, 2008, 1053–1061

A Modified Moist Ageostrophic $\boldsymbol{Q}$ Vector

YUE Caijun*[1,2] (岳彩军) and SHOU Shaowen[3] (寿绍文)

[1] *Shanghai Typhoon Institute, China Meteorological Administration, Shanghai* 200030

[2] *Laboratory of Typhoon Forecast Technique/China Meteorological Administration, Shanghai* 200030

[3] *School of Atmospheric Sciences, Nanjing University of Information Science and Technology, Nanjing* 210044

(Received 22 September 2007; revised 21 February 2008)

ABSTRACT

The quasi-geostrophic $\boldsymbol{Q}$ vector is an important diagnostic tool for studying development of surface rainfall associated with large-scale weather systems and is calculated using data at single vertical level. When ageostrophic $\boldsymbol{Q}$ vector was introduced, it required data at two vertical levels. In this study, moist ageostrophic $\boldsymbol{Q}$ vector is modified so that it can be calculated using data at a single vertical level. The comparison study between the original and modified moist ageostrophic $\boldsymbol{Q}$ vectors is conducted using the data from 5 to 6 July 1991 during the torrential rainfall event associated with the Changjiang-Huaihe mei-yu front in China. The results reveal that divergences of original and modified moist ageostrophic $\boldsymbol{Q}$ vectors have similar horizontal distributions and their centers are almost located in the precipitation centers. This indicates that modified moist ageostrophic $\boldsymbol{Q}$ vector can be used to diagnose convective development with reasonable accuracy.

Key words: moist ageostrophic $\boldsymbol{Q}$ vector, modification, latent heating, torrential rainfall associated with mei-yu front

Citation: Yue, C. J., and S. W. Shou, 2008: A modified moist ageostrophic $\boldsymbol{Q}$ vector. *Adv. Atmos. Sci.*, **25**(6), 1053–1061, doi: 10.1007/s00376-008-1053-x.

1. Introduction

The torrential rainfall and associated cloud development are associated with an ascending motion. The ascending motion is an important dynamic condition for condensation and precipitation processes, vertical heat and momentum transports, and conversion from potential energy to kinetic energy. Thus, the ascending motion is one of the most important processes associated with formation and development of severe weather. However, the ascending motion is not a conventional quantity and cannot be directly obtained from observations. Hoskins et al. (1978) introduced quasi-geostrophic $\boldsymbol{Q}$ vector, which is a unique forcing in the equation, and calculated this vector using single vertical level observational data. Once $\boldsymbol{Q}$ vector is calculated, the vertical velocity can be derived in a diagnostic way, which easily becomes operational (Dunn, 1991). Since then, the $\boldsymbol{Q}$ vector has been studied intensively (Keyser et al., 1988, 1992; Davies-Jones, 1991; Xu, 1992; Kurz, 1992; Barnes and Colman, 1993, 1994; Schar and Wernli, 1993; Jusem and Atlas, 1998; Martin, 1999a,b, 2006, 2007; Morgan, 1999; Donnadille et al., 2001; Lynch et al., 2003; Yue et al., 2003b; Jurewicz and Evans, 2004; Pyle et al., 2004; Brennan and Lackmann, 2006; Atallah et al., 2007; Thomas and Martin, 2007; Yue et al., 2007a) in various forms including generalized $\boldsymbol{Q}$ vector (Davies-Jones, 1991), $\boldsymbol{C}$ vector (Xu, 1992), semi-geostrophic $\boldsymbol{Q}$ vector (Li and Li, 1997), ageostrophic $\boldsymbol{Q}$ vector (Zhang, 1999), and moist ageostrophic $\boldsymbol{Q}$ vector (Zhang, 1998; Yao and Yu, 2000, 2001; Yao et al., 2004). The $\boldsymbol{Q}$ vector has successfully been applied to study torrential rainfall, typhoons, heavy snow, and dust storms.

The progress of $\boldsymbol{Q}$ vector studies were made after the concept of moist ageostrophic $\boldsymbol{Q}$ vector was introduced (Zhang, 1998; Yao and Yu, 2000, 2001; Yao et al., 2004) and was theoretically investigated (Yue et al., 2003c; Liu et al., 2007; Gao, 2007; Yang et al., 2007). Zhang (1998) first obtained the moist ageostrophic $\boldsymbol{Q}$ vector from the primitive equa-

*Corresponding author: YUE Caijun, yuecaijun2000@163.com

tions that contain large-scale latent heating associated with water vapor condensation. Yao and Yu (2000, 2001) and Yao et al. (2004) also derived similar moist ageostrophic $\boldsymbol{Q}$ vector from scale analysis. Yue et al. (2003c) modified the moist ageostrophic $\boldsymbol{Q}$ vector by including both large-scale and convective condensational heating processes. Recently, Liu et al. (2007) further modified the moist ageostrophic $\boldsymbol{Q}$ vector by including all heating sources such as large-scale and convective condensational heating, radiative heating, and sensible heating. Meanwhile, Yang et al. (2007) and Gao (2007) also derived the moist ageostrophic $\boldsymbol{Q}$ vector in a non-uniformly saturated, frictionless, moist adiabatic flow. The moist ageostrophic $\boldsymbol{Q}$ vector has been widely used to diagnose typhoons (e.g., Yao and Yu, 2000; Guo et al., 2005a; Yan and Cai, 2006) and torrential rainfall (e.g., Li et al., 2002; Liu et al., 2003; Guo et al., 2005b; Li et al., 2005; Liu, 2006). Yue et al. (2003b, 2007a) and Yang et al. (2006) conducted partitioning studies of moist ageostrophic $\boldsymbol{Q}$ vector. Yue et al. (2007b) applied moist ageostrophic $\boldsymbol{Q}$ vector to Quantitative Precipitation Forecast (QPF) for operational purposes.

The moist ageostrophic $\boldsymbol{Q}$ vector has similar advantages to the quasi-geostrophic $\boldsymbol{Q}$ vector, such as a unique forcing term in the equation and inclusion of diabatic heating, and the fact that it could be calculated with observational wind data (Yue et al., 2003a; Zhao et al., 2006), which is better than the quasi-geostrophic $\boldsymbol{Q}$ vector. However, the calculation of the moist ageostrophic $\boldsymbol{Q}$ vector needs multi-level data as well as multi-time data, which make the calculations complicated and inconvenient. The question is whether the moist ageostrophic $\boldsymbol{Q}$ vector can be modified so that it can be calculated using the single vertical-level data while it keeps all of the aforementioned advantages.

In this study, the moist ageostrophic $\boldsymbol{Q}$ vector is modified so that it can be calculated using data at a single vertical level. In the next section, the data will be briefly described. In section 3, the modified moist ageostrophic $\boldsymbol{Q}$ vector is derived and is compared with the original moist ageostrophic $\boldsymbol{Q}$ vector using the data from 5 to 6 July 1991 during the torrential rainfall associated with the Changjiang-Huaihe mei-yu front in China. A summary is given in section 4.

2. Data

A torrential rainfall event associated with the Changjiang-Huaihe mei-yu front occurred from 2000 LST 5 to 2000 LST 6 July 1991. The rainfall reached a peak at 0800 LST 6 July 1991 when a mei-yu front cyclone formed (Fig. 1). The surface rainfall increases

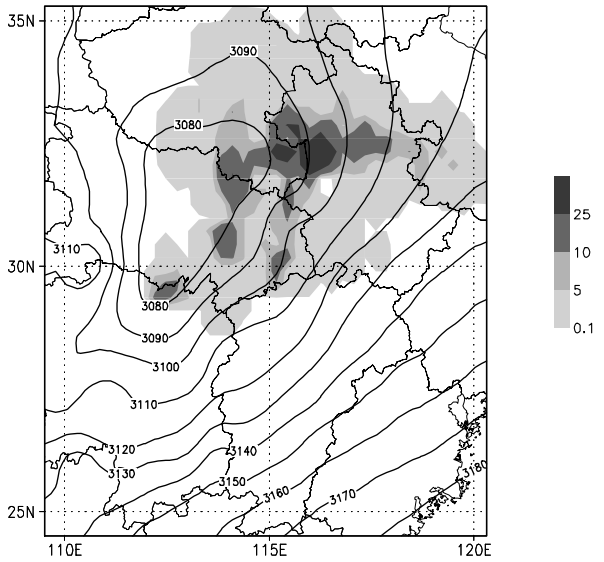

Fig. 1. Geopotential height (contour, gpm) at 700 hPa, 0800 LST 6 July 1991 and 1-hour (from 0700 to 0800 LST 6 July 1991) surface accumulated rainfall amount (shaded, mm).

dramatically with a banded structure and the rain rate may be higher than 30 mm h^{-1}. The detailed discussions of this torrential rainfall event can be found in Tao and Huang (1994), Shou and Li (1999), Shou et al. (2001), Liu et al. (2003), and Yue et al. (2003b, 2007a). The real data is conducted with the objective analysis, specifically, the horizontal resolution of the data is 30 km×30 km, and the vertical resolution is 50 hPa between 500 hPa and 1000 hPa and 100 hPa between 100 hPa and 500 hPa. The analysis focuses on the rainfall area of (29.25°–34.80°N, 109.72°–120.33°E).

3. The modification of moist ageostrophic $\boldsymbol{Q}$ vector

Following Zhang (1998), Yao and Yu (2000, 2001) and Yao et al. (2004), a moist ageostrophic $\boldsymbol{Q}$ vector ($\boldsymbol{Q}^*$ vector) can be expressed by

$$\boldsymbol{Q}^* = Q_x^* \boldsymbol{i} + Q_y^* \boldsymbol{j} \,, \tag{1}$$

$$Q_x^* = \frac{1}{2}\left[f\left(\frac{\partial v}{\partial p}\frac{\partial u}{\partial x} - \frac{\partial u}{\partial p}\frac{\partial v}{\partial x}\right) - \frac{R_d}{p}\left(\frac{\partial u}{\partial x}\frac{\partial T}{\partial x} + \frac{\partial v}{\partial x}\frac{\partial T}{\partial y}\right) + \frac{\partial H}{\partial x}\right] , \tag{1a}$$

$$Q_y^* = \frac{1}{2}\left[f\left(\frac{\partial v}{\partial p}\frac{\partial u}{\partial y} - \frac{\partial u}{\partial p}\frac{\partial v}{\partial y}\right) - \frac{R_d}{p}\left(\frac{\partial u}{\partial y}\frac{\partial T}{\partial x} + \frac{\partial v}{\partial y}\frac{\partial T}{\partial y}\right) + \frac{\partial H}{\partial y}\right] . \tag{1b}$$

Here, u and v are zonal and meridional components of wind, T is the temperature, and p is the pressure; The Coriolis parameter f is assumed to be constant;

$$H = \frac{R_d}{c_p \cdot p} H_s \,,$$

H_s is large-scale latent heating and is calculated by following Eq. (7), and R_d and c_p are the gas constant and specific heat at constant pressure for dry air, respectively; subscripts x and y denote zonal and meridional components, respectively. When large-scale latent heating is not included, $\boldsymbol{Q}^*$ vector is degraded to a dry $\boldsymbol{Q}^*$ vector, which can be written as

$$\boldsymbol{Q}^* = Q_x^* \boldsymbol{i} + Q_y^* \boldsymbol{j} \,, \tag{2}$$

$$Q_x^* = \frac{1}{2}\left[f\left(\frac{\partial v}{\partial p}\frac{\partial u}{\partial x} - \frac{\partial u}{\partial p}\frac{\partial v}{\partial x}\right) - \frac{R_d}{p}\left(\frac{\partial u}{\partial x}\frac{\partial T}{\partial x} + \frac{\partial v}{\partial x}\frac{\partial T}{\partial y}\right)\right] , \tag{2a}$$

$$Q_y^* = \frac{1}{2}\left[f\left(\frac{\partial v}{\partial p}\frac{\partial u}{\partial y} - \frac{\partial u}{\partial p}\frac{\partial v}{\partial y}\right) - \frac{R_d}{p}\left(\frac{\partial u}{\partial y}\frac{\partial T}{\partial x} + \frac{\partial v}{\partial y}\frac{\partial T}{\partial y}\right)\right] . \tag{2b}$$

Note that Eqs. (1) and (2) require data at two vertical levels.

Dutton (1976) found that the replacement of vertical wind shear with vertical shear of geostrophic wind is better than the replacement of wind by geostrophic wind, i.e.,

$$\frac{\partial u}{\partial p} \approx \frac{\partial u_{\rm g}}{\partial p} \,, \tag{3a}$$

$$\frac{\partial v}{\partial p} \approx \frac{\partial v_{\rm g}}{\partial p} \,, \tag{3b}$$

Thus, a modified moist ageostrophic $\boldsymbol{Q}$ vector ($\boldsymbol{Q}^\sharp$ vector) can be expressed by

$$\boldsymbol{Q}^\sharp = Q_x^\sharp \boldsymbol{i} + Q_y^\sharp \boldsymbol{j} \,, \tag{4}$$

$$Q_x^\sharp = \frac{1}{2}\left[-\frac{2R_d}{p}\left(\frac{\partial u}{\partial x}\frac{\partial T}{\partial x} + \frac{\partial v}{\partial x}\frac{\partial T}{\partial y}\right) + \frac{\partial H}{\partial x}\right] , \tag{4a}$$

$$Q_y^\sharp = \frac{1}{2}\left[-\frac{2R_d}{p}\left(\frac{\partial u}{\partial y}\frac{\partial T}{\partial x} + \frac{\partial v}{\partial y}\frac{\partial T}{\partial y}\right) + \frac{\partial H}{\partial y}\right] , \tag{4b}$$

where relations that

$$f v_{\rm g} = \frac{\partial \varphi}{\partial x} \,, f u_{\rm g} = -\frac{\partial \varphi}{\partial y} \,,$$

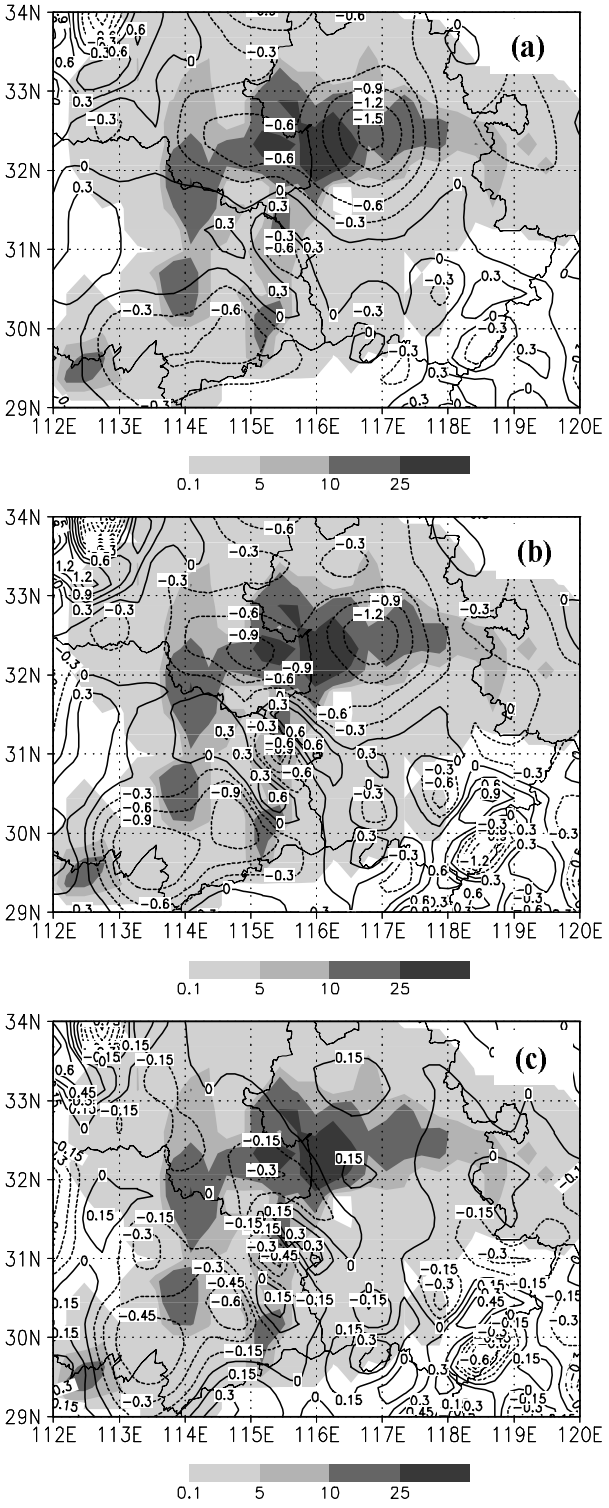

Fig. 2. (a) $2\nabla \cdot \boldsymbol{Q}^*$ calculated using Eq. (2) and (b) $2\nabla \cdot \boldsymbol{Q}^\sharp$ calculated using Eq. (5) and (c) their difference (10^{-15} hPa^{-1} s^{-3}) calculated using the data averaged from 850 to 500 hPa at 0800 LST 6 July 1991. The contour interval is 0.3×10^{-15} hPa^{-1} s^{-3} in (a) and (b) and 0.15×10^{-15} hPa^{-1} s^{-3} in (c). Surface rainfall amount (mm) is shaded.

and

$$\frac{\partial \varphi}{\partial p} = -\frac{R_d T}{p}$$

are used in the derivation of Eq. (4), meanwhile, large-scale latent heating H_s is calculated by following Eq. (8). Therefore, the calculation of $\boldsymbol{Q}^\sharp$ vector only needs data at a single vertical level, which is a similar advantage to what the quais-geostrophic $\boldsymbol{Q}$ vector has (Hoskins et al., 1978).

When large-scale latent heating is not included, $\boldsymbol{Q}^\sharp$ vector is degraded to a dry $\boldsymbol{Q}^\sharp$ vector, which can be written as

$$\boldsymbol{Q}^\sharp = Q_x^\sharp \boldsymbol{i} + Q_y^\sharp \boldsymbol{j} \,, \tag{5}$$

$$Q_x^\sharp = -\frac{R_d}{p}\left(\frac{\partial u}{\partial x}\frac{\partial T}{\partial x} + \frac{\partial v}{\partial x}\frac{\partial T}{\partial y}\right) \,, \tag{5a}$$

$$Q_y^\sharp = -\frac{R_d}{p}\left(\frac{\partial u}{\partial y}\frac{\partial T}{\partial x} + \frac{\partial v}{\partial y}\frac{\partial T}{\partial y}\right) \,, \tag{5b}$$

The ω equation can be symbolically written as

$$\nabla_h^2(\sigma\omega) + f\frac{\partial^2 \omega}{\partial p^2} = -2\nabla_h \cdot \boldsymbol{Q} \,. \tag{6}$$

To $\boldsymbol{Q}^*$, Eq. (6) can be expressed by

$$\begin{aligned}\nabla_h^2(\sigma\omega) + f\frac{\partial^2 \omega}{\partial p^2} = &-\frac{\partial}{\partial x}\left[f\left(\frac{\partial v}{\partial p}\frac{\partial u}{\partial x} - \frac{\partial u}{\partial p}\frac{\partial v}{\partial x}\right) - \frac{R_d}{p}\left(\frac{\partial u}{\partial x}\frac{\partial T}{\partial x} + \frac{\partial v}{\partial x}\frac{\partial T}{\partial y}\right) - \frac{\partial}{\partial x}\left(\frac{LR_d\omega}{c_p \cdot p}\frac{\partial q_s}{\partial p}\right)\right] \\ &-\frac{\partial}{\partial y}\left[f\left(\frac{\partial v}{\partial p}\frac{\partial u}{\partial y} - \frac{\partial u}{\partial p}\frac{\partial v}{\partial y}\right) - \frac{R_d}{p}\left(\frac{\partial u}{\partial y}\frac{\partial T}{\partial x} + \frac{\partial v}{\partial y}\frac{\partial T}{\partial y}\right) - \frac{\partial}{\partial y}\left(\frac{LR_d\omega}{c_p \cdot p}\frac{\partial q_s}{\partial p}\right)\right] \,.\end{aligned} \tag{6a}$$

To $\boldsymbol{Q}^\sharp$, Eq. (6) can be expressed by

$$\begin{aligned}\nabla_h^2(\sigma\omega) + f\frac{\partial^2 \omega}{\partial p^2} = &-\frac{\partial}{\partial x}\left\{-\frac{2R_d}{p}\left(\frac{\partial u}{\partial x}\frac{\partial T}{\partial x} + \frac{\partial v}{\partial x}\frac{\partial T}{\partial y}\right) - \frac{\partial}{\partial x}\left[\frac{LR_d\omega[a(273.16-b)R_dT(1+0.61q_s) - c_p(T-b)^2]q_s}{c_p[a(273.16-b)Lq_s + c_p(T-b)^2]p^2}\right]\right\} \\ &-\frac{\partial}{\partial y}\left\{-\frac{2R_d}{p}\left(\frac{\partial u}{\partial y}\frac{\partial T}{\partial x} + \frac{\partial v}{\partial y}\frac{\partial T}{\partial y}\right) - \frac{\partial}{\partial y}\left[\frac{LR_d\omega[a(273.16-b)R_dT(1+0.61q_s) - c_p(T-b)^2]q_s}{c_p[a(273.16-b)Lq_s + c_p(T-b)^2]p^2}\right]\right\}\end{aligned} \tag{6b}$$

4. Results

We first calculate divergences of dry $\boldsymbol{Q}^*$ and $\boldsymbol{Q}^\sharp$ ($2\nabla\cdot\boldsymbol{Q}^*$ and $2\nabla\cdot\boldsymbol{Q}^\sharp$) using Eqs. (2) and (5). Both show similarities as indicated by Fig. 2. The divergences of dry $\boldsymbol{Q}^*$ and $\boldsymbol{Q}^\sharp$ cover the rain area and their maxima are located around (32.5°N, 116.7°E), which is 0.5° away from the rainfall center at (32.5°N, 116.2°E). The difference between the divergences of dry $\boldsymbol{Q}^*$ and $\boldsymbol{Q}^\sharp$ is small over the major rain area to the north of 31°N (Fig. 2c). The large difference to the south of 31°N is due to that $|2\nabla \cdot \boldsymbol{Q}^\sharp| > |2\nabla \cdot \boldsymbol{Q}^*|$. Thus, the dry $\boldsymbol{Q}^\sharp$ accurately account for the dry $\boldsymbol{Q}^*$.

Before calculating $\boldsymbol{Q}^\sharp$ and $\boldsymbol{Q}^*$ using Eqs. (1) and (4), the latent heating term H is discussed. Since the vertical advection of saturated water vapor is significantly larger than the horizontal advection, latent heating term H_s can be expressed by

$$H_s \approx -L\omega\frac{\partial q_s}{\partial p} \,. \tag{7}$$

Following Ding (1989) and Zhang (1998), H_s becomes

$$H_s = -\frac{L\omega[a(273.16-b)R_dT(1+0.61q_s) - c_p(T-b)^2]q_s}{[a(273.16-b)Lq_s + c_p(T-b)^2]p^2} \,. \tag{8}$$

Here, $a = 17.1543, b = 36$. Thus, the calculation of H_s using Eq. (8) only requires data at a single vertical level. The specific derivation of Eq. (8) can be seen in the Appendix A.

Figure 3a shows similarity in the latent heating terms using Eqs. (7) and (8). Calculations using Eqs. (7) and (8) are nearly identical above 700 hPa whereas the latent heating calculated with the simplified method of Eq. (8) is smaller than that calculated with Eq. (7) below (Fig. 3b). Note that the latent

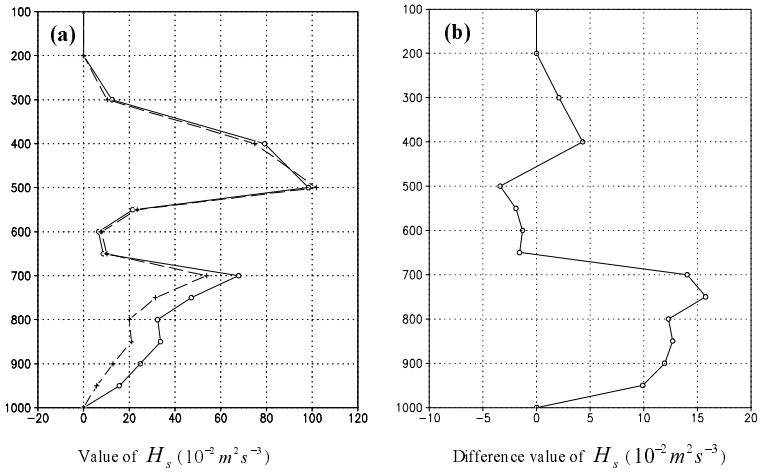

Fig. 3. (a) Vertical profiles of H_s calculated using Eqs. (7) (solid) and (8) (dashed) and (b) their difference at 0800 LST 6 July 1991. Units: 10^{-2} m^2 s^{-3}.

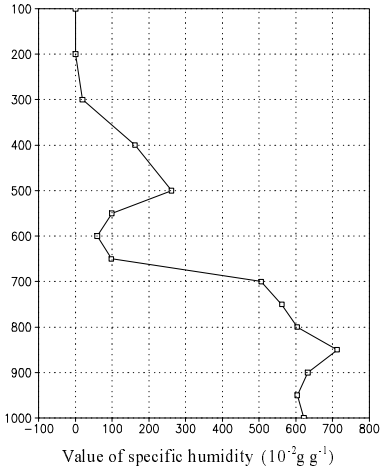

Fig. 4. Vertical profile of specific humidity (10^{-2} g g^{-1}) at 0800 LST 6 July 1991.

heating at 1000 hPa calculated using Eqs. (7) and (8) are zero because a vertical velocity of zero is assumed. Since the horizontal distributions of the latent heating term calculated using Eqs. (7) and (8) are similar (not shown), and the latent heating comes from the saturation of water vapor, the difference may be accounted for by the vertical profile of specific humidity. The specific humidity is much larger below 700 hPa than that above 700 hPa (Fig. 4). Thus, a large specific humidity could cause a difference in the latent heating calculated by Eqs. (7) and (8). Calculations of the Laplace term of latent heating

$$\frac{R_d}{c_p \cdot p}\nabla_h^2(H_s)$$

using Eqs. (7) and (8) and data at 700 hPa show similar horizontal distribution, and major negative areas are located over the areas with rain rates higher than 10 mm h^{-1} (Fig. 5). This suggests that the simplified method for the calculation of latent heating using the data at a single vertical level produces as good of a calculation of the Laplace term of latent heating as the method using the data at two vertical levels.

The divergences of moist $\boldsymbol{Q}^*$ and $\boldsymbol{Q}^\sharp$ ($2\nabla \cdot \boldsymbol{Q}^*$ and $2\nabla \cdot \boldsymbol{Q}^\sharp$) are calculated using Eqs. (1) and (4) (Fig. 6), and those of dry $\boldsymbol{Q}^*$ and $\boldsymbol{Q}^\sharp$ are computed using Eqs. (2) and (5) (Fig. 2). Figures 6 and 2 reveal similar horizontal distributions but with different magnitudes. From the paper, the divergences of moist $\boldsymbol{Q}$ vector should have two terms, the divergences of dry $\boldsymbol{Q}$ vector (Fig. 2) and the Laplace term of latent heating (Fig. 5). So the similar horizontal distributions of moist $\boldsymbol{Q}^*$ and $\boldsymbol{Q}^\sharp$ to those of dry $\boldsymbol{Q}^*$ and $\boldsymbol{Q}^\sharp$ suggest the dominance of dynamic and thermodynamic processes in the divergences of moist $\boldsymbol{Q}^*$ and $\boldsymbol{Q}^\sharp$ associated with the rainfall event during the front development. Meanwhile, the divergences of moist $\boldsymbol{Q}^*$ and $\boldsymbol{Q}^\sharp$ calculated with Eqs. (1) and (4) are generally larger than those of dry $\boldsymbol{Q}^*$ and $\boldsymbol{Q}^\sharp$ computed using Eqs. (2) and (5), which indicate that the effects of large-scale latent heating can't be avoided.

5. Summary

A modified moist ageostrophic $\boldsymbol{Q}$ vector is derived and calculated using single vertical level data during the torrential rainfall event associated with the Changjiang-Huaihe mei-yu front system in China from 5 to 6 July 1991. The calculation of modified moist ageostrophic $\boldsymbol{Q}$ vector is compared with the original moist ageostrophic $\boldsymbol{Q}$ vector. The results show that

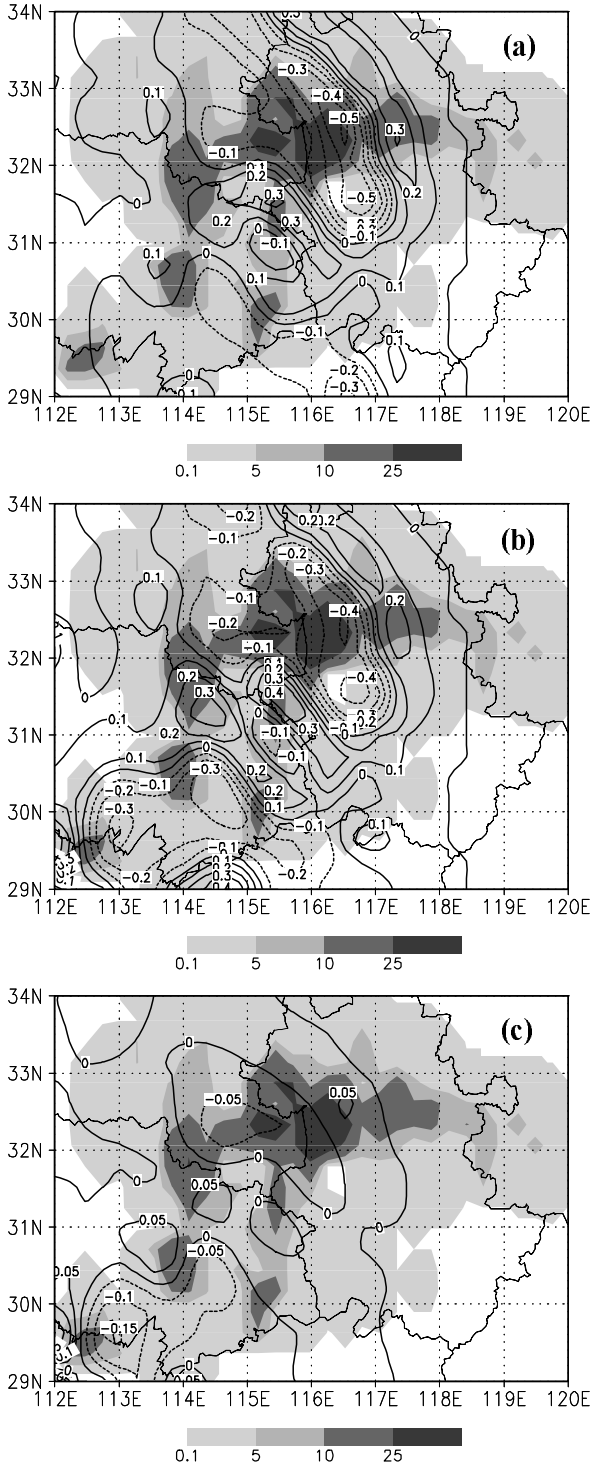

Fig. 5. (a) $(R_d/c_p \cdot p)\nabla_h^2(H_s)$ calculated using Eq. (7) and (b) $(R_d/c_p \cdot p)\nabla_h^2(H_s)$ calculated using Eq. (8) and (c) their difference (10^{-15} hPa^{-1} s^{-3}) calculated using the data at 700 hPa at 0800 LST 6 July 1991. The contour interval is 0.1×10^{-15} hPa^{-1} s^{-3} in (a) and (b) and 0.05×10^{-15} hPa^{-1} s^{-3} in (c). Surface rainfall amount (mm) is shaded.

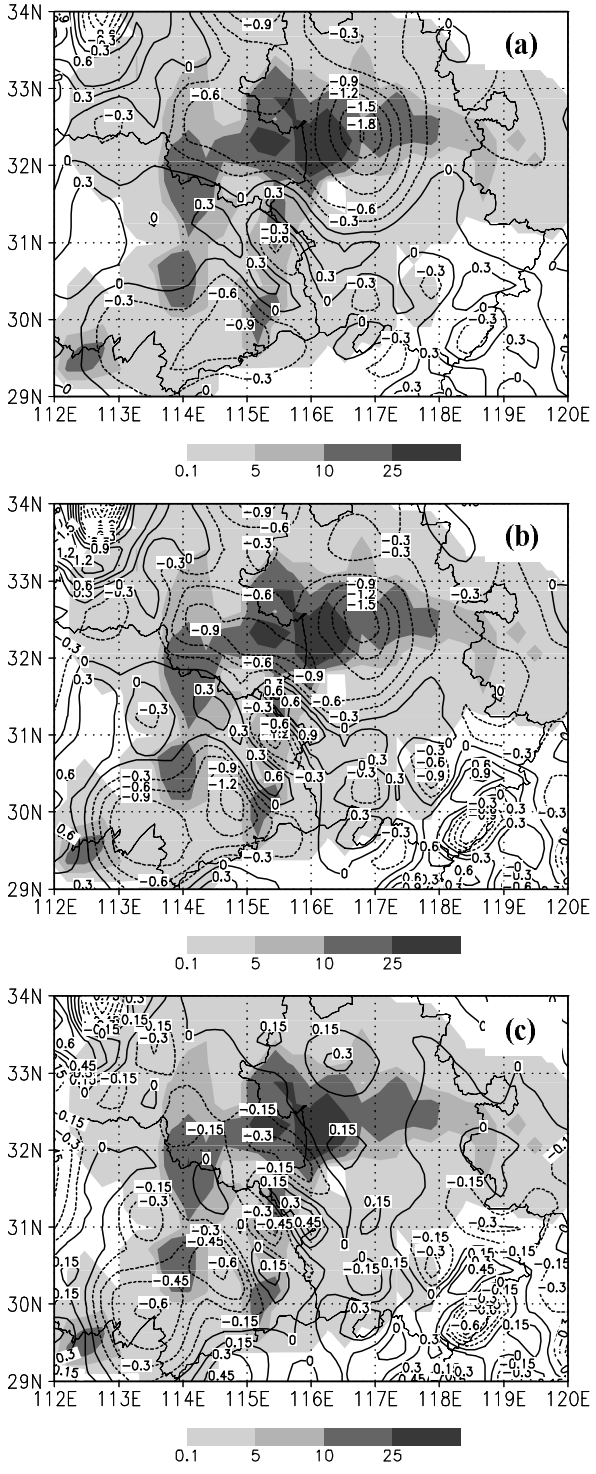

Fig. 6. (a) $2\nabla \cdot \boldsymbol{Q}^*$ calculated using Eq. (1) and (b) $2\nabla \cdot \boldsymbol{Q}^\sharp$ calculated using Eq. (4) and (c) their difference (10^{-15} hPa^{-1} s^{-3}) calculated using the data averaged from 850 to 500 hPa at 0800 LST 6 July 1991. The contour interval is 0.3×10^{-15} hPa^{-1} s^{-3} in (a) and (b) and 0.15×10^{-15} hPa^{-1} s^{-3} in (c). Surface rainfall amount (mm) is shaded.

the divergences of the original and modified dry ageostrophic $\boldsymbol{Q}$ vector show similar horizontal distributions in which their maxima occur near the centers of surface rainfall and that their maxima are collocated. The vertical profiles of large-scale latent heating using the original and modified formulations are identical above 700 hPa and their differences appear below 700 hPa. The differences are caused by large specific humidity. The Laplace of large-scale latent heating calculated using original and modified formulations also displays similarities. Therefore, the horizontal distribution of the divergence of the modified moist ageostrophic $\boldsymbol{Q}$ vector is similar to that of the original moist ageostrophic $\boldsymbol{Q}$ vector. This indicates that modified moist ageostrophic $\boldsymbol{Q}$ vector can be used to study convective development without loss of accuracy.

Acknowledgements. This research is supported by National Natural Science Foundation of China (Grant Nos. 40405009, 40075009, 40205008), Shanghai Typhoon Research Funding (Grant No. 2003ST005), Shanghai Weather Bureau Research Funding (No. 04A06), and Jiangsu Key Laboratory of Meteorological Disaster Funding (No. KJS0602). We appreciate the constructive comments and suggestions provided by the two anonymous reviewers, which improve this paper greatly.

APPENDIX A

Calculation of large-scale condensational heating rate (Ding, 1989; Zhang, 1998)

Large-scale condensational heating rate H_s can be expressed by

$$H_s = -L\frac{dq_s}{dt} \approx -L\omega\frac{dq_s}{dp} , \tag{A1}$$

where

$$q_s = 0.622\frac{e_s}{p} , \tag{A1a}$$

$$e_s = 6.11\exp\left[\frac{a(T-273.16)}{T-b}\right] , \tag{A1b}$$

$a = 17.1543$, and $b = 36$.

∂(A1a)/∂p leads to

$$\frac{\partial q_s}{\partial p} = q_s\left(-\frac{1}{p} + C\cdot\frac{\partial T}{\partial p}\right) . \tag{A2}$$

In the derivation of (A2), the relation that

$$\frac{\partial e_s}{\partial p} = e_s\cdot C\cdot\frac{\partial T}{\partial p} ,$$

where

$$C = \frac{a(273.16-b)}{(T-b)^2}$$

is used. $\partial q_s/\partial p$ is a vertical slope along a moist adiabatic saturated specific humidity. Due to the conservation of moist static energy along a moist adiabatic curve, we have

$$E_s = gz_s + c_pT + Lq_s . \tag{A3}$$

∂(A3)/∂p yields

$$\frac{\partial T}{\partial p} = \frac{R_dT_v}{c_pp} - \frac{L}{c_p}\frac{\partial q_s}{\partial p} , \tag{A4}$$

where $T_v = T(1+0.61q_s)$.

Substituting (A4) into (A2) leads to

$$\frac{\partial q_s}{\partial p} = \frac{(CR_dT_v - c_p)q_s}{(CLq_s + c_p)p} . \tag{A5}$$

With (A5), H_s becomes

$$H_s \approx -L\omega\frac{(CR_dT_v - c_p)q_s}{(CLq_s + c_p)p}$$

$$= -\frac{L\omega[a(273.16-b)R_dT(1+0.61q_s) - c_p(T-b)^2]q_s}{[a(273.16-b)Lq_s + c_p(T-b)^2]p} . \tag{A6}$$

REFERENCES

Atallah, E., L. F. Bosart, and A. R. Aiyyer. 2007: Precipitation distribution associated with landfalling tropical cyclone over the eastern United States. *Mon. Wea. Rev.*, **135**, 2185–2206.

Barnes, S. L., and B. R. Colman, 1993: Quasigeostrophic diagnosis of cyclogenesis associated with a cut off extratropical cyclone—The Christmas 1987 storm. *Mon. Wea. Rev.*, **121**, 1613–1634.

Barnes, S. L., and B. R. Colman, 1994: Diagnosing an operational numerical model using $\boldsymbol{Q}$-vector and potential vorticity concepts. *Wea. Forecasting*, **9**, 85–102.

Brennan, M. J., and G. M. Lackmann, 2006: Observation diagnosis and model forecast evaluation of unforecasted incipient precipitation during the 24–25 January 2000 east coast cyclone. *Mon. Wea. Rev.*, **134**, 2033–2054.

Davies-Jones, R., 1991: The frontogenetical forcing of secondary circulations. Part I: the duality and generalization of the $\boldsymbol{Q}$ vector. *J. Atmos. Sci.*, **48**, 497–509.

Ding, Y., 1989: *Diagnostic and Analytical Methods in Synoptic Dynamics*. Science Press, Beijing, 114–116. (in Chinese)

Donnadille, J., J.-P. Cammas, P. Mascart, and D. Lambert, 2001: FASTEX IOP 18: A very deep tropopause fold. II: Quasi-geostrophic omega diagnoses. *Quart. J. Roy. Meteor. Soc.*, **127**, 2269–2286.

Dunn, L. B., 1991: Evaluation of vertical motion: Past, Present, and Future. *Wea. Forecasting*, **6**, 65–73.

Dutton, J. A., 1976: *The Ceaseless Wind*. McGraw-Hill, 579pp.

Gao, S., 2007: *Dynamical Basis and Forecast Methods of Atmospheric Meso-scale Motion*. China Meteorological Press, Beijing, 191–200. (in Chinese)

Guo, R., Y. Lu, Y. Li, Y. Hai, and M. Gao, 2005a: Analyses of a Yunnan rainstorm process influenced by the "Imbudo" typhoon. *Plateau Meteorology*, **24**, 784–791. (in Chinese)

Guo, R., Y. Li, X. Yang, and C. Zhou, 2005b: Non-geostrophic wet $\boldsymbol{Q}$-vector analysis and application of heavy precipitation in winter in Yunnan. *Meteorological Monthly*, **31**, 12–16. (in Chinese)

Hoskins, B. J., I. Dagbici, and H. C. Darics, 1978: A new look at the ω-equation. *Quart. J. Roy. Metor. Soc.*, **104**, 31–38.

Jurewicz, M. L., and M. S. Evans. 2004: A comparison of two banded, heavy snowstorms with very different synoptic settings. *Wea. Forecasting*, **19**, 1011–1028.

Jusem, J. C., and R. Atlas, 1998: Diagnostic evaluation of vertical motion forcing mechanism by using $\boldsymbol{Q}$-vector partitioning. *Mon. Wea. Rev.*, **126**, 2166–2184.

Keyser, D., M. J. Reeder, and R. J. Reed, 1988: A generalization of Petterssen's frontogenesis function and its relation to the forcing of vertical motion. *Mon. Wea. Rev.*, **116**, 762–780.

Keyser, D., B. D. Schmidt, and D. G. Duffy, 1992: Quasi-geostrophic vertical motions diagnosed from along- and cross-isentrope components of the $\boldsymbol{Q}$ vector. *Mon. Wea. Rev.*, **20**, 731–741.

Kurz, M., 1992: Synoptic diagnosis of frontogenetic and cyclogenetic processes. *Meteorology and Atmospheric Physics*, **48**, 77–91.

Li, B., and G. Li, 1997: Application of the semi-geostrophic $\boldsymbol{Q}$ vector in study of the mei-yu front heavy rain. *Atmospheric Science Research and Application*, **12**, 31–38. (in Chinese)

Li, Y., T. Zhang, and R. Guo, 2002: Ageostrophic wet $\boldsymbol{Q}$ vector analysis of a persistent rainstorm process in Yunnan. *Journal of Nanjing Institute of Meteorology*, **25**, 259–264. (in Chinese)

Li, Y., L. Ji, X. Pan, and Y. Li, 2005: Analysis by diagnosis of wet $\boldsymbol{Q}$ vector of a rainstorm process. *Scientia Meteorologica Sinica*, **25**, 179–185. (in Chinese)

Liu, Y., 2006: Wet $\boldsymbol{Q}$-vector analysis of a continued heavy rain process over the eastern Qinghai-Xizang plateau. *Meteorological Monthly*, **32**, 43–49. (in Chinese)

Liu, H., S. Shou, and J. Zhou, 2007: Improvement and application of ageostrophic wet $\boldsymbol{Q}$-vector. *Journal of Nanjing Institute of Meteorology*, **30**, 86–93. (in Chinese)

Liu, Z., C. Yue, S. Shou, and M. Dong, 2003: Using wet $\boldsymbol{Q}$ vector to diagnose a process of mei-yu front heavy rain. *Journal of Nanjing Institute of Meteorology*, **26**, 102–110. (in Chinese)

Lynch, A. H., E. N. Cassano, J. J. Cassano, and L. R. Lestak. 2003: Case studies of high wind events in Barrow, Alaska: Climatological context and development processes. *Mon. Wea. Rev.*, **131**, 719–732.

Martin, J. E., 1999a: Quasi-geostrophic forcing of ascent in the occluded sector of cyclones and the trowal airstream. *Mon. Wea. Rev.*, **127**, 70–88.

Martin, J. E., 1999b: The separate roles of geostrophic vorticity and deformation in the midlatitude occlusion process. *Mon. Wea. Rev.*, **127**, 2404–2418.

Martin, J. E., 2006: The role of shearwise and transverse quasigeostrophic vertical motions in the midlatitude cyclone life cycle. *Mon. Wea. Rev.*, **134**, 1174–1193.

Martin, J. E., 2007: Lower-tropospheric height tendencies associated with the shearwise and transverse components of quasigeostrpphic vertical motion. *Mon. Wea. Rev.*, **135**, 2803–2809.

Morgan, M. C., 1999: Using piecewise potential vorticity inversion to diagnose frontogenesis. Part I: A partitioning of the $\boldsymbol{Q}$ vector applied to diagnosing surface frontogenesis and vertical motion. *Mon. Wea. Rev.*, **127**, 2796–2821.

Pyle, M. E., D. Keyser, and L. F. Bosart, 2004: A diagnostic study of jet streaks: Kinematic signatures and relationship to coherent tropopause disturbances. *Mon. Wea. Rev.*, **132**, 297–319.

Schar, C., and H. Wernli, 1993: Structure and evolution of an isolated semi-geostrophic cyclone. *Quart. J. Roy. Meteor. Soc.*, **119**, 57–90.

Shou, S., and Y. Li, 1999: Study on moist potential vorticity and symmetric instability during a heavy rain event occurred in the Jiang-Huai valleys. *Adv. Atmos. Sci.*, **16**, 314–321.

Shou, S., Y. Li, and K. Fan, 2001: Isentropic potential vorticity analysis of the mesoscale cyclone development in a heavy rain process. *Acta Meteorologica Sinica*, **59**, 560–568. (in Chinese)

Tao, Z., and W. Huang, 1994: 3-D trajectory analysis of air parcel associated with high and low level jets in heavy rain. *Acta Meteorologica Sinica*, **52**, 359–367. (in Chinese)

Thomas, B. C., and J. E. Martin, 2007: A synoptic climatology and composite analysis of the Alberta Clipper. *Wea. Forecasting*, **22**, 315–333.

Xu, Q., 1992: Ageostrophic pseudovorticity and geostrophic $\boldsymbol{C}$-vector forcing—A new look at $\boldsymbol{Q}$ vector in three dimensions. *J. Atmos. Sci.*, **49**, 981–990.

Yan, Q., and Q. Cai, 2006: Application of ageostrophic wet $\boldsymbol{Q}$-vector analysis in torrential rain of typhoon "Rananim". *Journal of Tropical Meteorology*, **22**, 505–509. (in Chinese)

Yang, S., S. Gao, and D. Wang, 2007: Diagnostic analyses of the ageostrophic $\boldsymbol{Q}$ vector in the non-uniformly saturated, frictionless, and moist adiabatic flow. *J. Geophys. Res.*, **112**(D09114), 1–9, doi:10.1029/2006JD008142.

Yang, X., T. Shen, H. Liu, D. Xue, and F. Wan, 2006: Application of the wet $\boldsymbol{Q}$ vector partitioning method to the diagnosis of the heavy rainstorm. *Plateau Meteorology*, **25**, 464–475. (in Chinese)

Yao, X., and Y. Yu, 2000: Non-geostrophic wet $\boldsymbol{Q}$-vector

analysis and its application to typhoon torrential rain. *Acta Meteorologica Sinica*, **58**, 436–446. (in Chinese)

Yao, X., and Y. Yu, 2001: Perfect $\boldsymbol{Q}$-vector and its diagnoses. *Plateau Meteorology*, **20**, 208–213. (in Chinese)

Yao, X., Y. Yu, and S. Shou, 2004: Diagnostic analyses and application of the moist ageostrophic $\boldsymbol{Q}$ vector. *Adv. Atmos. Sci.*, **21**, 96–102.

Yue, C., S. Shou, and M. Dong, 2003a: Quantitative analysis of several $\boldsymbol{Q}$ vectors. *Journal of Applied Meteorological Science*, **14**, 39–48. (in Chinese)

Yue, C., S. Shou, K. Lin, and X. Yao, 2003b: Diagnosis of the heavy rain near a mei-yu front using the wet $\boldsymbol{Q}$ vector partitioning method. *Adv. Atmos. Sci.*, **20**, 37–44.

Yue, C., Y. Shou, and S. Shou, 2003c: The improvement and perfection of $\boldsymbol{Q}$ vector. *Journal of Tropical Meteorology*, **19**, 308–316. (in Chinese)

Yue, C., M. Dong, S. Shou, and X. Yao, 2007a: Improved wet $\boldsymbol{Q}$ vector's analytical method and the mechanism of mei-yu front rainstorm genesis. *Plateau Meteorology*, **26**, 165–175. (in Chinese)

Yue, C., Y. Shou, S. Shou, G. Zeng and Y. Wang, 2007b: Study on wet $\boldsymbol{Q}$ vector interpretation technique with its application to quantitative precipitation forecast (QPF). *Journal of Applied Meteorological Science*, **18**, 666–675. (in Chinese)

Zhang, X., 1998: An expression of the wet $\boldsymbol{Q}$ vector and application. *Meteorological Monthly*, **24**, 3–7. (in Chinese)

Zhang, X., 1999: The expression of the modified $\boldsymbol{Q}$ vector and its application. *Journal of Tropical Meteorology*, **15**, 162–167. (in Chinese)

Zhao, G., L. Cheng, and X. Li, 2006: Comparison and application of $\boldsymbol{Q}$-vector and wet-$\boldsymbol{Q}$-vector to diagnosis of storm rain. *Meteorological Monthly*, **32**, 25–30. (in Chinese)